Inorganic Chemistry

Article

pubs.acs.org/IC

Hydrothermal Synthesis of Single-Crystalline Perovskite $PbTiO_3$ Nanosheets with Dominant (001) Facets

Shiqi Deng, Gang Xu,* Huiwen Bai, Lingling Li, Shan Jiang, Ge Shen, and Gaorong Han

State Key Laboratory of Silicon Materials, Department of Materials Science and Engineering, and Key Laboratory of Advanced Materials and Applications for Battery of Zhejiang Province, Zhejiang University, Hangzhou 310027, China

Supporting Information

ABSTRACT: Single-crystalline tetragonal perovskite lead titanate ($PbTiO_3$) nanosheets with dominant (001) facets have been successfully synthesized by employing layered $K_2Ti_6O_{13}$ nanofibers as titanium sources. The as-prepared $PbTiO_3$ nanosheets were characterized by means of X-ray diffraction, field-emission scanning electron microscopy, transmission electron microscopy (TEM), high-resolution TEM, and selected-area electron diffraction. In order to understand the formation mechanism of the $PbTiO_3$ nanosheets, a series of time-dependent experiments were performed. Because of the substitution of Pb^{2+} ions for K^+ ions, the TiO_6 octahedral lamellas exfoliate from the layered $K_2Ti_6O_{13}$ crystal structure. Then the exfoliated TiO_6 octahedral lamellas as templates transform to lamellar $PbTiO_3$ species by reacting with the dehydrated Pb^{2+} ions. With hydrothermal treatment prolongation, the lamellar $PbTiO_3$ species crystallize to single-crystalline $PbTiO_3$ nanosheets. Moreover, the thickness of the synthesized single-crystalline $PbTiO_3$ nanosheets can be tailored in the range of 10−50 nm by controlling the hydrothermal treatment time. In addition, the band gap and the optoelectronic properties of the single-crystalline $PbTiO_3$ nanosheets are investigated by UV−vis absorption and photoluminescence.

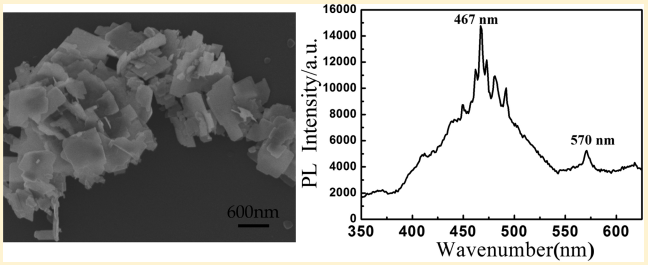

INTRODUCTION

Below the Curie temperature, ferroelectric oxides exhibit spontaneous polarization that can be reoriented with the external electric field. Because the two stable polarization states correspond to the positive and negative electric bias, ferroelectric oxides have received considerable attention in nonvolatile memory devices.[1−5] Previous research works performed by Park and co-workers have demonstrated that the perovskite $BaTiO_3$ nanowires with a diameter size as small as 10 nm still retain ferroelectricity.[6] Although 10^9 bit/cm^2 can be achieved based on the $BaTiO_3$ nanowires, it is still necessary to pursue nonvolatile ferroelectric random-access memories (NVFRAMs) with much higher storage density to meet the practice requirements of miniaturization. Whereas two-dimensional (2D) nanostructures can have high tap density by overlapping assembly compared to one-dimensional (1D) nanostructures, it is a prospective to fabricate NVFRAMs with much higher storage density by perovskite ferroelectric nanosheets.

However, synthesis of the perovskite oxide nanosheets is a challenge because of the less anisotropic crystal lattice structure. Because the semiconductor nanocrystals were found to have excellent properties compared to their bulk counterpart,[7,8] current worldwide intense researches on nanomaterials have been initiated. As an important kind of ferroelectric material, perovskite oxide nanostructures also have attracted considerable attention. In spite of the weak anisotropism in the lattice structure, a lot of perovskite oxide 1D nanostructures have been realized by bottom-up chemical methods.[9] An early paper reporting on the perovskite oxide 1D nanostructures was proposed by Park and co-workers, in which the $BaTiO_3$ and $SrTiO_3$ nanowires are realized by solution-phase decomposition of bimetallic alkoxide precursors in the presence of coordinating ligands.[10] After a while, a more suitable method was proposed in our previous research works.[11] By virtue of the preferential adsorption of the organic modifiers on the (100) and (010) planes, $PbZr_{0.52}Ti_{0.48}O_3$ nanorods and nanowires were obtained. Using the layered alkali titanate nanofibers as templates, $BaTiO_3$ and $PbTiO_3$ nanorods have also been prepared by the hydrothermal route and low-temperature molten salt method, respectively.[12−14] With regard to the ferroelectric perovskite oxide nanosheets, however, only $PbTiO_3$ nanosheets with a size of about 10 nm thickness were reported in our more recent work.[15] The preferential fast combination of Na^+ or K^+ ions with the O^{2-} ions situated on the (001) or (111) surfaces results in $PbTiO_3$ nanosheets with dominant (001) or (111) facets. Nonetheless, accompanying the formation of $PbTiO_3$ nanosheets, a lot of $PbTiO_3$ nanoparticles are also obtained.

Since the discovery of graphenes,[16,17] increasing attention has been paid to 2D nanostructures because of their unique properties and potential applications. Because the nanosheets well reflect the intrinsic symmetry of the layered lattice structures, to date a variety of layered metal oxides,[18−20]

Received: May 22, 2014
Published: September 29, 2014

   dx.doi.org/10.1021/ic501180g | Inorg. Chem. 2014, 53, 10937−10943

chalcogenides,[21,22] and hydroxides[23] have been exfoliated into nanosheets by chemical or physical methods. Potassium titanate $K_2Ti_6O_{13}$ is a layered lattice structure. Although synthesized $K_2Ti_6O_{13}$ is generally made of nanofibers,[24−28] it is argued that during the hydrothermal treatment the formed $K_2Ti_6O_{13}$ species first crystallize to nanosheets, which reflect the intrinsic symmetry of the layered lattice and then roll to nanofibers. Moreover, many experiments have demonstrated that the K^+ ions inserted among the TiO_6 octahedral layers in the titanate crystal structures are easily exchanged with H^+ and other metal ions.[24,25] Therefore, the $K_2Ti_6O_{13}$ nanofibers are widely used as titanium sources to synthesize titanium-based compound nanocrystals.[12−14,29−33] For example, because of exchange of Ba^{2+} and Pb^{2+} ions with the inserted K^+ ions, the $BaTiO_3$[12] and $PbTiO_3$ nanorods[13,14] are synthesized by the hydrothermal route and low-temperature molten salt method with the layered potassium titanate nanofibers as templates, respectively. More recently, in our group $PbTiO_3$ perovskite nanoplates with a thickness of above 100 nm are hydrothermally synthesized with $K_2Ti_6O_{13}$ nanofibers as titanium sources under the effect of the NaOH high concentrations, in which the formed lead oxide nanoplates in advance are argued to play an important role in the formation of the $PbTiO_3$ nanoplates.[33] Nonetheless, it should be noticed that all of the synthesized titanium-based nanostructures are scarcely nanosheets.

Lead titanate ($PbTiO_3$) is a prototypical perovskite ferroelectric oxide. Below a temperature of about 490 °C, $PbTiO_3$ crystals display spontaneous polarization. Thus, $PbTiO_3$ is a promising candidate for NVFRAMs. Herein, we report a novel approach to synthesizing the single-crystalline tetragonal perovskite $PbTiO_3$ nanosheets in high yield. In order to realize the $PbTiO_3$ nanosheets, the synthesized layered $K_2Ti_6O_{13}$ nanofibers in advance are used as titanium sources. During the hydrothermal treatment, the substitution of Pb^{2+} ions for the K^+ ions makes the TiO_6 octahedral lamella exfoliated from the $K_2Ti_6O_{13}$ lattice structure and transformed to lamellar $PbTiO_3$ species. These special lamellar $PbTiO_3$ species further crystallize to the single-crystalline tetragonal perovskite $PbTiO_3$ nanosheets with dominant (001) facets. The band gap and the optoelectronic properties of the single-crystal tetragonal perovskite $PbTiO_3$ nanosheets are characterized by UV−vis absorption and photoluminescence (PL).

EXPERIMENTAL SECTION

The hydrothermal treatment was carried out in a homemade Teflon-lined stainless steel autoclave. All of the chemicals used in this work, including tetrabutyl titanate [$(C_4H_9O)_4Ti$], lead nitrate [$Pb(NO_3)_2$], potassium hydroxide (KOH), ethanol, and ammonia, were of analytical-grade purity and were used as received without further purification. Distilled water was used in the preparation of all aqueous solutions.

The layered potassium titanate $K_2Ti_6O_{13}$ nanofibers used as titanium sources for the hydrothermal synthesis of single-crystalline $PbTiO_3$ nanosheets were first prepared by hydrothermally treating the suspension of titanium hydroxide precipitates with a KOH concentration of 10 mol/L at 200 °C for 16 h. The titanium hydroxide precipitates were prepared by introducing the ammonia solution to the ethanol/$(C_4H_9O)_4Ti$ solution under continuous magnetic stirring. After filtering and washing with distilled water six times, the titanium hydroxide precipitates were dispersed in distilled water with vigorous magnetic stirring, followed by the addition of KOH pellets, forming a titanium hydroxide precipitate suspension with a high KOH concentration of 10 mol/L for the hydrothermal treatment. In a typical procedure for the synthesis of single-crystalline $PbTiO_3$ nanosheets, the as-prepared $K_2Ti_6O_{13}$ nanofibers were dispersed in distilled water with vigorous magnetic stirring, followed by the addition of $Pb(NO_3)_2$ and KOH pellets. After continuous magnetic stirring for 6 h, the suspension was adjusted to 40 mL and poured into a 50 mL stainless steel Teflon-lined autoclave for hydrothermal treatment. In the final feedstock suspension, a Pb^{2+} ion concentration of 0.2 mol/L, a Pb/Ti molar ratio of 1:1, and a KOH concentration of 10 mol/L were created. The hydrothermal treatment was performed by placing the sealed autoclave in an oven and keeping it at 200 °C for 24 h, and then the autoclave was cooled to room temperature in air. The products were filtered and washed several times, first with distilled water and then with absolute ethanol, and finally oven-dried in air at 60 °C for 24 h. In order to investigate the formation mechanism of the single-crystalline $PbTiO_3$ nanosheets, the hydrothermal treatment time was adjusted in the range of 0.5−32 h, and other hydrothermal treatment conditions were riveted.

Powder X-ray diffraction (XRD) patterns were obtained by a Rigaku D/max-RA X-ray diffractometer with high-intensity Cu Ka (λ = 1.5418 Å) radiation with a step size of 0.02°. Scanning elelctron microscopy (SEM) measurements and energy-dispersive spectroscopy (EDS) were performed using a Hitachi S-4800 microscope (Japan). Transmission electron microscopy (TEM and STEM) images were taken with a FEI Tecnai G2 F30 transmission electron microscope at 160 kV, and high-resolution TEM (HRTEM) images were caught at 200 kV. The optical adsorption spectrum was measure by a Hitachi model U-4100 UV−vis spectrometer. PL spectral measurements were done with a Shimadzu RF-5301 spectrofluorimeter.

RESULTS AND DISCUSSION

Figure 1 shows the XRD pattern and SEM image of the hydrothermally synthesized $K_2Ti_6O_{13}$ nanofibers. All of the

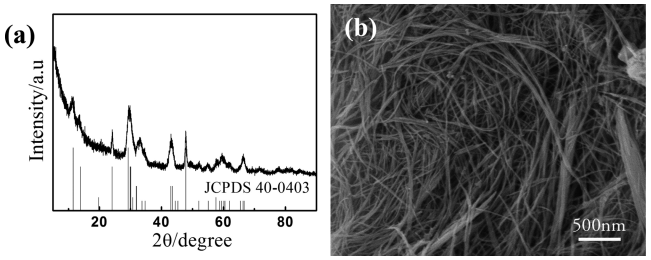

Figure 1. (a) XRD pattern and (b) SEM image of the hydrothermally synthesized $K_2Ti_6O_{13}$ nanofibers.

diffraction peaks shown in Figure 1a are well indexed to the monoclinic lattice of $K_2Ti_6O_{13}$ (JCPDS no. 40-0403), indicating that the obtained products after hydrothermal treatment of the titanium hydroxide precipitate under the effect of a high KOH concentration are pure $K_2Ti_6O_{13}$ with a layered lattice structure. The SEM image presented in Figure 1b reveals that the obtained $K_2Ti_6O_{13}$ samples consist entirely of nanofibers, agreeing well with that reported in lectures.[24−28]

Figure 2 shows the XRD pattern of the samples hydrothermally synthesized with the $K_2Ti_6O_{13}$ nanofibers as titanium sources. All of the diffraction peaks can be indexed to the tetragonal $PbTiO_3$ perovskite with the lattice parameters of a = b = 0.3899 nm and c = 0.4153 nm, corresponding well with the reported data of JCPDS no. 06-0452, implying that the as-prepared samples are of pure crystalline $PbTiO_3$ with tetragonal perovskite structure. The strong and sharp reflection peaks indicate that the as-prepared $PbTiO_3$ products are well crystallized. However, observed in detail, one can find that the (001) diffraction peak becomes abnormally higher than the (100) diffraction peak, which is opposite to the traditional literature values (JCPDS no. 06-0425), suggesting that higher

dx.doi.org/10.1021/ic501180g | Inorg. Chem. 2014, 53, 10937−10943

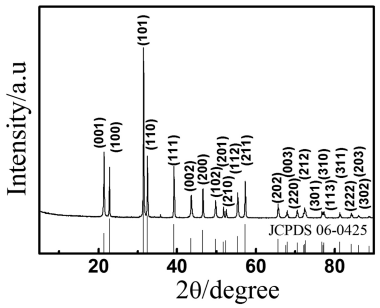

Figure 2. XRD pattern of the samples hydrothermally synthesized with the $K_2Ti_6O_{13}$ nanofibers as titanium sources.

amounts of (001) planes contribute to the XRD in the as-prepared $PbTiO_3$ products.

The SEM image of the as-prepared $PbTiO_3$ samples is shown in Figure 3a. Evidently, the as-prepared $PbTiO_3$ samples

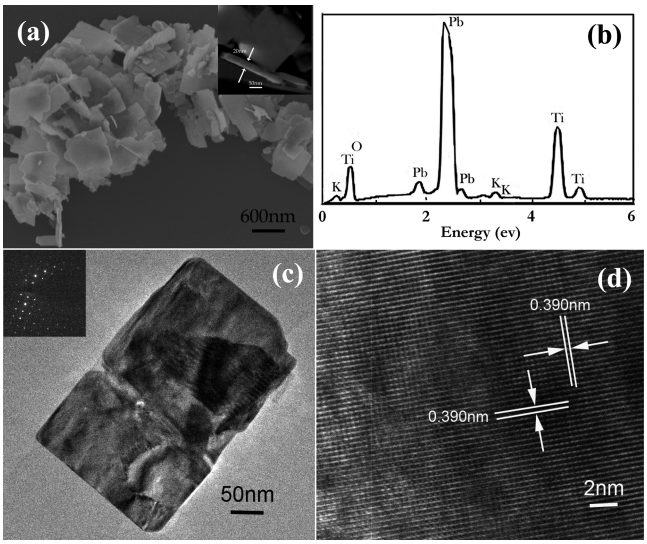

Figure 3. (a) SEM image, (b) EDS spectrum, (c) TEM image, and (d) HRTEM image of the hydrothermally synthesized $PbTiO_3$ nanosheets. The inset in part a is the STEM image of one standing $PbTiO_3$ nanosheet, and the inset in part c shows the SAED pattern caught from the corresponding whole single $PbTiO_3$ nanosheet.

entirely consist of nanosheets with a thickness of ca. 20 nm (see the inset in Figure 3a) and a lateral size of 500−800 nm. The corresponding EDS spectrum shown in Figure 3b indicates that the nanosheets consist of lead, titanium, and oxygen with a ratio of about 1:1:3, agreeing well with the nominal chemical composition of the $PbTiO_3$ perovskite. The $PbTiO_3$ nanosheets were further characterized by TEM and HRTEM. Representative TEM and HRTEM images of a single $PbTiO_3$ nanosheet are presented in parts c and d of Figure 3, respctively. Two sets of lattice fringes with 0.390 intervals, which agree well with the spacing of the (100) and (010) planes, are identified from the HRTEM image shown in Figure 3d. Moreover, the selected-area electron diffraction (SAED) pattern (the inset in Figure 3c) caught from the corresponding whole single $PbTiO_3$ nanosheets is regular and can be indexed as the incident electron beam parallel to the [001] direction. It is argued that the as-prepared $PbTiO_3$ nanosheets are single-crystalline and dominated with (001) facets. Therefore, the intensity of the (001) diffraction peak enhances abnormally higher than the (100) diffraction peak of the as-prepared $PbTiO_3$ nanosheets, opposite to the traditional literature values (JCPDS no. 06-0425; Figure 2).

In order to investigate the formation mechanism of the single-crystalline tetragonal perovskite $PbTiO_3$ nanosheets, a set of time-dependent experiments were carried out by changing the hydrothermal treatment time. The samples obtained at different stages of the hydrothermal treatment were characterized by XRD and SEM, respectively. Figure 4

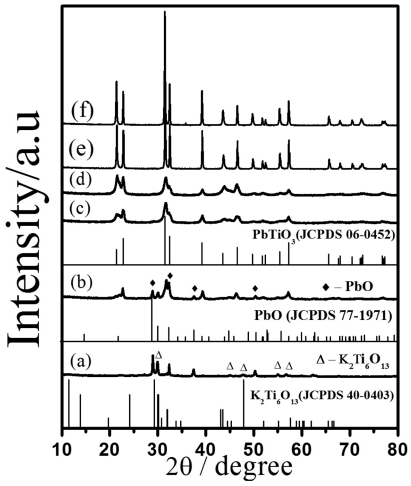

Figure 4. XRD patterns of the samples obtained after hydrothermal treatment for different times: (a) 0.5, (b) 2, (c) 6, (d) 16, (e) 24, and (f) 32 h.

shows the XRD patterns of the samples obtained by the hydrothermal treatment at 200 °C for 0.5, 2, 6, 16, 24, and 32 h. When the hydrothermal treatment time is less than 0.5 h, the $PbTiO_3$ perovskite is hardly detected from the obtained samples; only PbO and $K_2Ti_6O_{13}$ are identified out. With the reaction time is prolonged to 2 h, the diffraction peaks of PbO and $K_2Ti_6O_{13}$ decline and simultaneously the $PbTiO_3$ perovskite phase is found. When the hydrothermal treatment time is further extended to over 6 h, all of the diffraction peaks of the obtained samples can be indexed to the tetragonal $PbTiO_3$ perovskite (JCPDS no. 06-0452) and without any PbO and $K_2Ti_6O_{13}$. Moreover, with prolongation of the hydrothermal treatment time from 6 to 32 h, the diffraction peaks accordingly become sharp and intense, implying that the synthesized $PbTiO_3$ perovskite crystals grow larger. Otherwise, when the hydrothermal treatment time is extended to over 16 h, the intensity of the (001) peak becomes abnormally higher than that of the (100) peak, reflecting the higher amount of $PbTiO_3$ nanosheet formation. There is an additional small peak at around 35° in the XRD pattern of the samples synthesized for 32 h, revealing that a few impurities form, accompanying the $PbTiO_3$ nanosheets at this moment.

Figure 5 presents the SEM images of the obtained samples after hydrothermal treatment for different times. One can find that, with formation of the tetragonal perovskite $PbTiO_3$, the morphology of the obtained samples gradually changes from nanofibers to nanosheets. With regard to the samples obtained by hydrothermal treatment for 0.5 h, predominant nanofibers are observed, reflecting the morphology of the $K_2Ti_6O_{13}$ precursors (Figure 5a). Wheres at this time a small amount of PbO is identified by XRD in the obtained samples and PbO easily crystallizes to nanosheets in aqueous solution, it can be

dx.doi.org/10.1021/ic501180g | Inorg. Chem. 2014, 53, 10937−10943

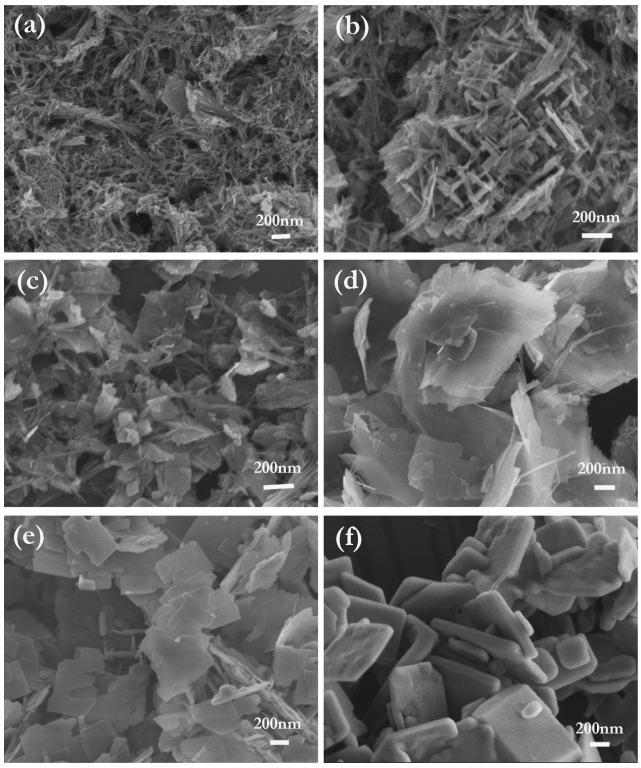

Figure 5. SEM images of the samples obtained after hydrothermal treatment for different times: (a) 0.5, (b) 2, (c) 6, (d) 16, (e) 24, and (f) 32 h.

suggested that the observed few nanosheets correspond to PbO formation. When the hydrothermal treatment time increases to 2 h, a higher number of nanosheets are observed but for the predominant $K_2Ti_6O_{13}$ nanofibers (Figure 5b). In view of formation of the $PbTiO_3$ perovskite and the decline of PbO (Figure 4b), the observed nanosheets at this time can be ascribed to the tetragonal perovskite $PbTiO_3$ nanosheets. As the hydrothermal treatment time extends to 6 h, the tetragonal perovskite $PbTiO_3$ nanosheets predominate over the obtained samples, while a few of the $K_2Ti_6O_{13}$ nanofibers are still found (Figure 5c). Nonetheless, because the diffraction intensity of $K_2Ti_6O_{13}$ is far smaller than that of $PbTiO_3$, some of titanate $K_2Ti_6O_{13}$ is not checked out by XRD (Figure 4c). With prolongation of the hydrothermal treatment time from 6 to 32 h, the $K_2Ti_6O_{13}$ nanofibers gradually disappear and pure tetragonal perovskite $PbTiO_3$ nanosheets are obtained (Figure 5c–f). Moreover, the $PbTiO_3$ nanosheets grow larger and thicker. Thus, the diffraction peaks of the $PbTiO_3$ perovskite become sharper and higher (Figure 4c–f). The abnormal enhancement of the (001) diffraction peak in the XRD pattern (Figure 4d–f) of the obtained samples after hydrothermal treatment for over 16 h can be ascribed to the predominant $PbTiO_3$ nanosheets.

Our previous research works have demonstrated that, with titanium hydroxide precipitates or commercial TiO_2 powders as titanium sources, the hydrothermally synthesized tetragonal perovskite $PbTiO_3$ samples are cubic particles, reflecting the intrinsic symmetry of the lattice.[34,35] In the present experiment, because of the use of the titanate $K_2Ti_6O_{13}$ nanofibers as titanium sources, the synthesized $PbTiO_3$ crystals change from cubic particles to single-crystal nanosheets. Therefore, it is believed that the used titanate $K_2Ti_6O_{13}$ nanofibers play an important role in synthesis of the singe-crystal tetragona perovskite $PbTiO_3$ nanosheets. The structural model of the layered $K_2Ti_6O_{13}$ compound is shown in Figure 6. In a

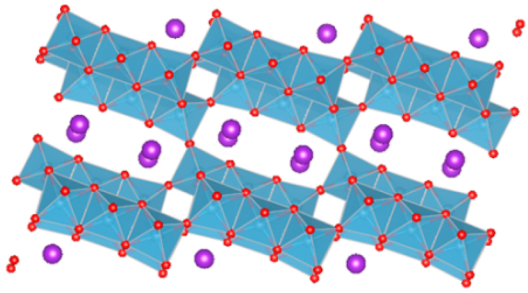

Figure 6. Structural models of $K_2Ti_6O_{13}$.

$K_2Ti_6O_{13}$ crystal, TiO_6 octahedra compose 2D layers by sharing edges and corners. The 2D TiO_6 octahedral layers link together by connecting the corners of the opposing octahedra. K^+ ions insert in the tunnels formed between the 2D TiO_6 octahedral layers. Many research reports have demonstrated that the alkali ions in titanate between the TiO_6 octahedral layers can be exchanged.[24,25] On the other hand, as the $Pb(NO_3)_2$ and KOH pellets are dissolved, in turn, in the suspension, in which the $K_2Ti_6O_{13}$ nanofibers were well dispersed, a lot of soluble $Pb(OH)_3^-$ ions form because of the high KOH concentration.[36] According to the oxide formation mechanism under hydrothermal conditions,[37] the soluble $Pb(OH)_3^-$ ions dehydrate and condense to $PbTiO_3$ perovskite crystals by reacting with the $K_2Ti_6O_{13}$ nanofibers. Whereas the radius of the Pb^{2+} ions (119 pm) is smaller than that of the K^+ ions (138 pm), it can be inferred that during the hydrothermal treatment the Pb^{2+} ions tend to diffuse into the tunnels of the $K_2Ti_6O_{13}$ structure and exchange with the K^+ ions under the effect of the high KOH concentration. When the substitution of Pb^{2+} ions for K^+ ions achieves a moderate extent, the layered titanate structure becomes unstable and some TiO_6 octahedral lamella exfoliate from the layered titanate structure by breaking the connecting corners of the opposing octahedra, which belong to the opposite TiO_6 octahedral layers. The exfoliated TiO_6 octahedral lamella as templates further react with the soluble $Pb(OH)_3^-$ ions to form lead titanate lamellar species by undergoing a dehydration and condensation process, in which the edge-shared TiO_6 octahedral lamella transform to corner-shared TiO_6 lamella in pursuit of more stability. Subsequently, the lead titanate lamellar species crystallize to single-crystal tetragonal perovskite $PbTiO_3$ nanosheets. Moreover, because the limitation along the normal direction of the nanosheets is less than that along the plane, the single-crystal tetragonal perovskite $PbTiO_3$ nanosheets are dominated with (001) facets (Figure 3c,d). Therefore, after hydrothermal treatment for 2 h, in the obtained samples, a few tetragonal perovskite $PbTiO_3$ nanosheets are observed, accompanying the predominant $K_2Ti_6O_{13}$ nanofibers (Figure 5b). With prolongation of the hydrothermal time from 2 to 16 h, the $PbTiO_3$ nanosheets gradually increase and grow larger; meanwhile, the $K_2Ti_6O_{13}$ nanofibers decrease (Figure 5b–d). When the hydrothermal time increases to 16 h, the obtained samples are only composed of $PbTiO_3$ nanosheets, whereas the precursor $K_2Ti_6O_{13}$ nanofibers are hardly observed. At this time, the synthesized $PbTiO_3$ nanosheets are irregular and very thin with a thickness of less than 10 nm (Figure 5d). After this moment, because the

dx.doi.org/10.1021/ic501180g | Inorg. Chem. 2014, 53, 10937–10943

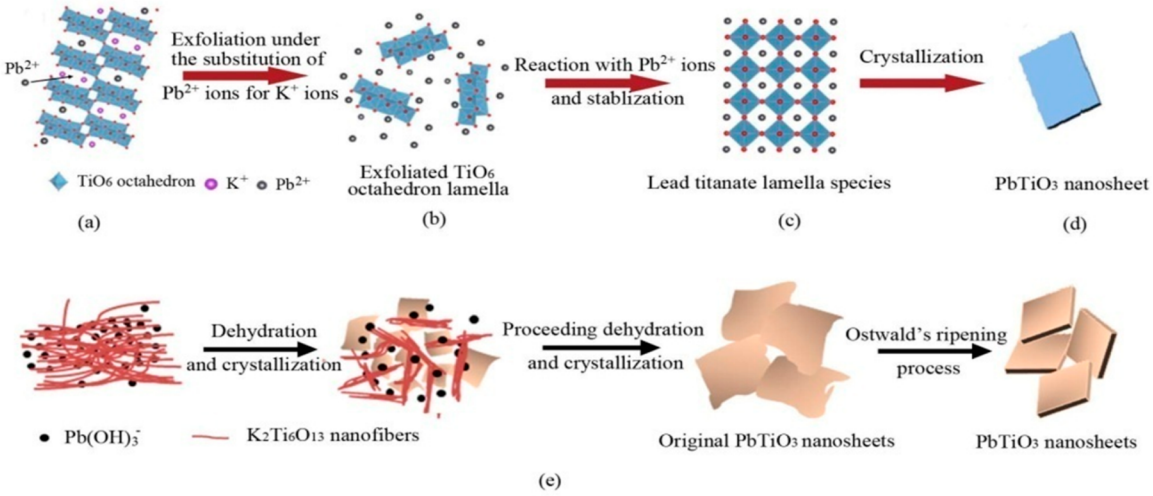

Figure 7. Schematic illustration of (a–d) the formation mechanism and (e) the hydrothermal synthesis process of the single-crystalline tetragonal perovskite $PbTiO_3$ nanosheets with layered $K_2Ti_6O_{13}$ nanofibers as titanium sources. (a) Pb^{2+} ions diffuse into the $K_2Ti_6O_{13}$ crystal structure and substitute for K^+ ions. (a and b) Because of the extensive substitution of Pb^{2+} ions for K^+ ions, a lot of edge-shared TiO_6 octahedral lamella exfoliate from the layered $K_2Ti_6O_{13}$ crystal structure. (b and c) In order to be more stable, the exfoliated TiO_6 octahedral lamella transform to lamellar lead titanate species with corner-shared TiO_6 octahedra by reacting with the dehydrated Pb^{2+} ions. (c and d) The lamellar lead titanate species crystallize to single-crystalline tetragonal perovskite $PbTiO_3$ nanosheets.

lead titanate species concentration around the lateral of the nanosheets is higher than that around the planes, an Ostwald ripening process occurs. With prolongation of the hydrothermal treatment time to 24 and 32 h, as a result, the irregular $PbTiO_3$ nanosheets grow thicker and of regular rectangular shape (Figure 5e,f). To summarize the discussion above, a scheme is simply depicted in Figure 7 for illustrating the formation mechanism and the formation process of the single-crystal tetragonal perovskite $PbTiO_3$ nanosheets. The above-proposed formation mechanism of the $PbTiO_3$ nanosheets is also confirmed by the another experimental research work (see the Supporting Information), in which, because of formation of the layered $K_2Ti_6O_{13}$ in advance under the high KOH concentration, the $PbTiO_3$ nanosheets form and self-assemble into three-dimensional flowerlike $PbTiO_3$ nanostructures. This research work will be reported elsewhere in the future.

However, at the initial stage of the hydrothermal treatment, because the Pb^{2+} ion diffusion and substitution for K^+ ions in the layered $K_2Ti_6O_{13}$ structure delay the formation of $PbTiO_3$, a lot of PbO forms by dehydration and condensation of some $Pb(OH)_3^-$ ions. Thus, in the samples obtained by hydrothermal treatment for 0.5 h, a few PbO are identified (Figure 4a). Whereas the dehydration of $Pb(OH)_3^-$ ions to PbO is reversible, because of the expense of $Pb(OH)_3^-$ ions for the formation of lead titanate, with prolongation of the hydrothermal treatment, the PbO formed gradually reverses to the $Pb(OH)_3^-$ ion and disappears (Figure 4a–c). Otherwise, upon prolongation of the hydrothermal treatment time to 32 h, because the dissolvability of lead hydroxide is larger than that of titanium hydroxide, a higher amount of Pb^{2+} ions dissolve in the reaction medium solvent from the formed $PbTiO_3$ perovskite lattice than titanium. As a consequence, a few titanium-rich lead titanate forms in the samples obtained after hydrothermal treatment for 32 h and is checked out by XRD (Figure 4f).

UV–vis absorption measurement was carried out to understand the energy structures and optical properties of the as-prepared $PbTiO_3$ nanosheets. Figure 8a shows the typical

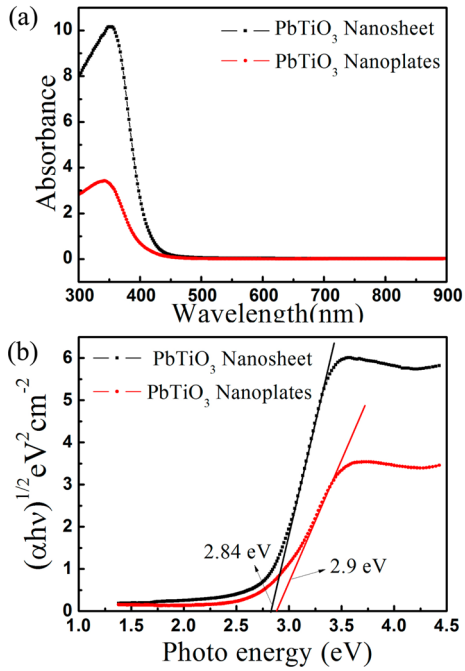

Figure 8. (a) UV–vis absorption spectra of as-prepared $PbTiO_3$ nanosheets and nanoplates. (b) Plots of $(\alpha h\nu)^{1/2}$ as a function of the photon energy for $PbTiO_3$ nanosheets and nanoplates.

UV–vis absorption spectra measured from the as-prepared single-crystalline $PbTiO_3$ nanosheets. As a control, the typical UV–vis absorption spectra were also measured from the $PbTiO_3$ nanoplates,[33] the thickness of which is over 100 nm, much larger than that of the as-prepared single-crystalline $PbTiO_3$ nanosheets. A strong absorption in the UV region associated with the band–band transition is clearly observed from both samples. However, an obvious red shift of the absorption edge occurs for the $PbTiO_3$ nanosheets compared to the $PbTiO_3$ nanoplates. The absorption edge for the $PbTiO_3$ nanosheets is about 412 nm, whereas that for the $PbTiO_3$

dx.doi.org/10.1021/ic501180g | Inorg. Chem. 2014, 53, 10937–10943

nanoplates is about 403 nm. Because the tetragonal perovskite $PbTiO_3$ is an indirect semiconductor,[38] the band gap of as-prepared $PbTiO_3$ nanosheets can be estimated from the intercept of the tangents to the plots of $(\alpha h\nu)^{1/2}$ versus photon energy $(h\nu)$. Figure 8b shows the plots of $(\alpha h\nu)^{1/2}$ versus $h\nu$, which is obtained on the basis of the UV−vis absorption spectra shown in Figure 8a. The estimated band gap of the single-crystalline $PbTiO_3$ nanosheets is about 2.84 eV, whereas that of the $PbTiO_3$ nanoplates is about 2.90 eV. Whereas the band gap of the single-crystalline $PbTiO_3$ nanosheets is much smaller than that reported (about 3.45 eV) for the $PbTiO_3$ crystals,[39] it can be argued that the density of the surface states in the $PbTiO_3$ nanosheets is relatively high and the interaction between the exciton and lattice phonon is very strong.[40] With increasing thickness, the density of the surface states would decrease. Thus, the band gap of the $PbTiO_3$ nanoplates is larger than that of the $PbTiO_3$ nanosheets. Whereas the electron and hole can be effectively trapped on the surface states and the charge separation would be effective,[41] the high PL emission of the $PbTiO_3$ nanosheets is prospective.

Figure 9 shows the PL emission spectra of the $PbTiO_3$ nanosheets and nanoplates with an excitation wavelength of

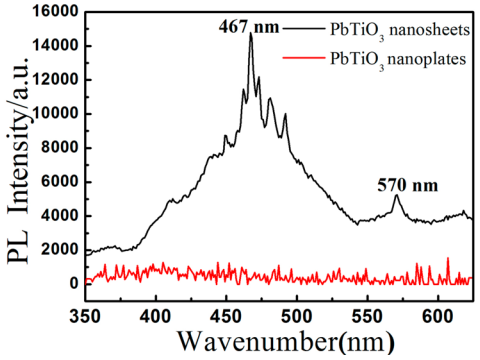

Figure 9. Room temperature PL spectra of $PbTiO_3$ nanosheets and nanoplates excited at 280 nm.

280 nm at room temperature. The $PbTiO_3$ nanosheets exhibit a strong structure surface-emission band around 467 nm with broad bands from 450 to 500 nm, confirming the presence of several surface states. Whereas the research work performed by Leite and co-workers has demonstrated that the $PbTiO_3$ powders with perfect crystal structure do not display any surface emmission, the strong emission of the $PbTiO_3$ nanosheets should be attributed to the recombination of electron−hole pairs trapped on the surface states. As for the surface-emission band around 570 nm, this can be ascribed to the recombination of the trapped electrons and holes located in the interfacial region between the crystalline and amorphous $PbTiO_3$ of the $PbTiO_3$ nanosheets.[42] Because of the decrease in the density of the surface states, the $PbTiO_3$ nanoplates with a size of above 100 nm thickness do not display any surface emission, similar to the $PbTiO_3$ powders with perfect crystal structure.[42]

CONCLUSION

Single-crystalline tetragonal perovskite $PbTiO_3$ nanosheets with dominant (001) facets were successfully synthesized via a conventional hydrothermal route by employing the layered $K_2Ti_6O_{13}$ nanofibers as titanium sources. The prepared single-crystal tetragonal perovksite $PbTiO_3$ nanosheets can be tailored in the thickness range of 10−50 nm by controlling the hydrothermal treatment time. During the hydrothermal treatment process, the Pb^{2+} ions diffuse into the layered $K_2Ti_6O_{13}$ structure and substitute for the K^+ ions under the effect of the high KOH concentration. As substitution of the Pb^{2+} ions for the K^+ ions accumulates to a moderate extent, the edge-shared TiO_6 octahedral lamella exfoliate from the layered $K_2Ti_6O_{13}$ lattice structure and the template transforms to lamellar $PbTiO_3$ species by reacting with the dehydrated Pb^{2+} ions. Then, with prolongation of the hydrothermal treatment, the lamellar $PbTiO_3$ species crystallize to single-crystalline $PbTiO_3$ nanosheets. Because of less limitation along the normal direction of the nanosheets, moreover, the synthesized single-crystalline $PbTiO_3$ nanosheets are dominated with (001) facets. In addition, the single-crystalline $PbTiO_3$ nanosheets with dominant (001) facets are a wide-band-gap semiconductor with a band gap of about 2.84 eV and exhibit strong PL emission in the visible range at room temperature. Because of the high tap density, the $PbTiO_3$ nanosheets could be a prospective candidate for nonvolatile memory devices, optoelectronics, piezoelectric sensors, and other microelectronic functional devices. From a more fundamental point of view, it is believed that the present reported study proposes a promising technique to prepare a 2D nanostructure with perovskite structure and may bring a lot of perovskite oxide ferroelectric nanosheets.

ASSOCIATED CONTENT

Supporting Information

Details of our other experimental research work, confirming our proposed formation mechanism of the $PbTiO_3$ nanosheets. This material is available free of charge via the Internet at http://pubs.acs.org.

AUTHOR INFORMATION

Corresponding Author

*E-mail: msegxu@zju.edu.cn.

Author Contributions

The manuscript was written through contributions of all authors. All authors have given approval to the final version of the manuscript.

Notes

The authors declare no competing financial interest.

ACKNOWLEDGMENTS

This work is supported by the National Natural Science Foundation of China, under Grants 61274004 and 51232006, and the Zhejiang Natural Science Foundation, China, under Grant LY12B07007.

REFERENCES

(1) Scott, J. F.; De Araujo, C. A. P. *Science* **1989**, *246*, 1400−1405.
(2) Scott, J. F. *Ferroelectr. Rev.* **1998**, *1*, 1.
(3) Park, B. H.; Kang, B. S.; Bu, S. D.; Noh, T. W.; Lee, J.; Jo, W. *Nature* **1999**, *401*, 682−684.
(4) Waser, R.; Rüdiger, A. *Nat. Mater.* **2004**, *3*, 81−82.
(5) Chu, M. W.; Szafraniak, I.; Scholz, R.; Harnagea, C.; Hesse, D.; Alexe, M.; Gösele, U. *Nat. Mater.* **2004**, *3*, 87−90.
(6) Yun, W. S.; Urban, J. J.; Gu, Q.; Park, H. *Nano Lett.* **2002**, *2*, 447−450.
(7) Leutwyler, W. K.; Bürgi, S. L.; Burgl, H. *Science* **1996**, *271*, 933−937.
(8) Heath, J. R. *Acc. Chem. Res.* **1999**, *32*, 388.

(9) Rørvik, P. M.; Grande, T.; Einarsrud, M. A. *Adv. Mater.* **2011**, *23*, 4007−4034.
(10) Urban, J. J.; Yun, W. S.; Gu, Q.; Park, H. K. *J. Am. Chem. Soc.* **2002**, *124*, 1186.
(11) Xu, G.; Ren, Z. H.; Du, P. Y.; Weng, W. J.; Shen, G.; Han, G. R. *Adv. Mater.* **2005**, *17*, 907−910.
(12) Kang, S. O.; Jang, H. S.; Kim, K. B.; Park, B. H.; Jung, M. J.; Kim, Y. I. *Mater. Res. Bull.* **2008**, *43*, 996−1003.
(13) Cai, Z. Y.; Xing, X. R.; Yu, R. B.; Sun, X. Y. *Inorg. Chem.* **2007**, *46*, 7423−7427.
(14) Rørvik, P. M.; Lyngdal, T.; Saeterli, R.; van Helvoort, A. T.; Holmestad, R.; Grande, T.; Einarsrud, M. A. *Inorg. Chem.* **2008**, *47*, 3173−3181.
(15) Xu, G.; Huang, X. Q.; Krstic, V.; Chen, S. Q.; Yang, X.; Chao, C. Y.; Shen, G.; Han, G. R. *CrystEngComm* **2014**, *16*, 4373.
(16) Novoselov, K. S.; Geim, A. K.; Morozov, S. V.; Jiang, D.; Zhang, Y.; Dubonos, S. V.; Firsov, A. A. *Science* **2004**, *306*, 666−669.
(17) Eda, G.; Chhowalla, M. *Adv. Mater.* **2010**, *22*, 2392−2415.
(18) Schaak, R. E.; Mallouk, T. E. *Chem. Mater.* **2002**, *14*, 1455−1571.
(19) Schaak, R. E.; Mallouk, T. E. *Chem. Commun.* **2002**, *7*, 706−707.
(20) Ma, R.; Sasaki, T. *Adv. Mater.* **2010**, *22*, 5082−5104.
(21) Zhang, K.; Kim, H. J.; Shi, X.; Lee, J. T.; Choi, J. M.; Song, M. S.; Park, J. H. *Inorg. Chem.* **2013**, *52*, 9807−9812.
(22) Coleman, J. N.; Lotya, M.; O'Neill, A.; Bergin, S. D.; King, P. J.; Khan, U.; Nicolosi, V. *Science* **2011**, *331*, 568−571.
(23) Ma, R.; Liu, Z.; Li, L.; Iyi, N.; Sasaki, T. *J. Mater. Chem.* **2006**, *16*, 3809−3813.
(24) Du, G. H.; Chen, Q.; Han, P. D.; Yu, Y.; Peng, L. M. *Phys. Rev. B* **2003**, *67*, 035323.
(25) Wang, R. H.; Chen, Q.; Wang, B. L.; Zhang, S.; Peng, L. M. *Appl. Phys. Lett.* **2005**, 133101.
(26) Menzel, R.; Peiró, A. M.; Durrant, J. R.; Shaffer, M. S. *Chem. Mater.* **2006**, *18*, 6059−6068.
(27) Kiatkittipong, K.; Ye, C.; Scott, J.; Amal, R. *Cryst. Growth Des.* **2010**, *10*, 3618−3625.
(28) Zhang, T.; Chen, Q.; Peng, L. M. *Adv. Funct. Mater.* **2008**, *18*, 3018−3025.
(29) Li, J. M.; Yang, H. L.; Li, Q.; Xu, D. S. *CrystEngComm* **2012**, *14*, 3019.
(30) Li, J. M.; Yu, Y. X.; Chen, Q. W.; Li, J. J.; Xu, D. S. *Cryst. Growth Des.* **2010**, *10*, 2111−2115.
(31) Deng, H.; Qiu, Y. C.; Yang, S. H. *J. Mater. Chem.* **2009**, *19*, 976−982.
(32) Han, X. G.; Wang, X.; Xie, S. F.; Kuang, Q.; Ouyang, J. J.; Xie, Z. X.; Zheng, L. S. *RCS Adv.* **2012**, *2*, 3251−3253.
(33) Chao, C. Y.; Ren, Z. H.; Yin, S. M.; Gong, S. Y.; Yang, X.; Xu, G.; Li, X.; Shen, G.; Han, G. R. *CrystEngComm* **2013**, *15*, 8036.
(34) Xu, G.; Jiang, W.; Qian, M.; Chen, X. X.; Li, Z. B.; Han, G. R. *Cryst. Growth Des.* **2009**, *9*, 13−16.
(35) Chao, C. Y.; Ren, Z. H.; Zhu, Y. H.; Xiao, Z.; Liu, Z. Y.; Xu, G.; Mai, J. Q.; Li, X.; Shen, G.; Han, G. R. *Angew. Chem., Int. Ed.* **2012**, *51*, 9283−9287.
(36) Inczedy, J. *Applications of complex equilibria*; Ellis Horwood: Chichester, U.K., 1976; p 323.
(37) Stambaugh, E. P. Hydrothermal precipitation of high-quality oxides. *Presented at the SME-AIME Fall Meeting*, St. Louis, MO, 1977.
(38) Hosseini, S. M.; Movlarooy, T.; Kompany, A. *Phys. B: Condens. Matter* **2007**, *391*, 316−321.
(39) Moret, M. P.; Devillers, M. A. C.; Wörhoff, K.; Larsen, P. K. *J. Appl. Phys.* **2002**, *92*, 468−474.
(40) Thomas, J.; Yoon, M. *Appl. Catal., B* **2012**, *111*, 502−508.
(41) Yoon, M.; Seo, M.; Jeong, C.; Jang, J. H.; Jeon, K. S. *Chem. Mater.* **2005**, *17*, 6069−6079.
(42) Leite, E. R.; Santos, L. P. S.; Carreno, N. L. V.; Longo, E.; Paskocimas, C. A.; Varela, J. A.; Pizani, P. S. *Appl. Phys. Lett.* **2001**, *78*, 2148−2150.